Heat Transfer Characterization of Flat Plain Fins and Round Tube Heat Exchangers

N. Kayansayan
Dokuz Eylül University,
Department of Mechanical Engineering,
İzmir, Turkey

■ The effects of outersurface geometry on the performance of flat plain fins and round tube crossflow heat exchangers are considered. With the finning parameter varying from 11 to 23, a total of 10 geometrically distinct configurations were tested over a Reynolds number range of 100–30,000. The tube outside diameter and collar thickness define the characteristic dimension. The convective heat transfer coefficients are presented as plots of the Colburn j factor versus Reynolds number and compare well with previous studies. The dispersion in the majority of the data is $\pm 10\%$. The j factor, Reynolds number, and finning parameter are correlated.

Keywords: *compact heat exchangers, fin-and-tube exchanger, forced convection*

INTRODUCTION

Heat exchangers with flat fins and round tubes are quite common in applications related to the air-conditioning, heating, and refrigeration industries. Owing to the complex pattern of fluid flow over the fin-and-tube surface, the theoretical prediction of heat transfer coefficients is often precluded. The combined process of heat and momentum transfer serves to complicate the analysis. Therefore, it is necessary to resort to experimentation in order to construct useful models.

A variety of flow configurations have been studied and documented in the literature. Reviews of the literature have been given by Webb [1] and McQuiston [2]. The results reported here, however, are unique in that the present study not only extends the range of the geometrical parameters of previous studies but also considers a larger Reynolds number range. The following review is not intended to be exhaustive, but rather to provide a background for the present study.

Rich [3, 4] examined the effects of fin spacing and number of tube rows on the heat transport of several heat exchangers. Varying the number of tube rows from one to six, Rich concluded that, depending upon the Reynolds number, the average heat transfer coefficient for a deep coil may be higher or lower than that for a shallow coil.

In the Colburn j-factor correlation presented by Elmahdy and Biggs [5], the Reynolds number exponent, m, was assumed to be a strong function of the physical parameters of the finned tube exchanger over the Reynolds number range 200–2000. Experiments were performed, and the m values for every individual exchanger with a specified geometry were determined by a regression analysis method.

McQuiston [6] developed a very simple correlation for four-row staggered banks with plain fins. It was found that the j-factors were best correlated by applying a multiplication factor to the Reynolds number given by $(A_o/A_{to})^n$. The Reynolds number in the analysis ranged between 100 and 4000.

The work now presented documents the average heat transfer coefficients for 10 distinct fin-tube-bank configurations obtained from controlled experiments in a wind tunnel. In the experiments, the number of tube rows along the flow direction was four, and the Reynolds number spanned the range from 10^2 to 3×10^4. The characteristic dimension is the tube outside diameter including the collar wall thickness. This choice makes it possible to correlate the heat transfer data in a compact form. Comparison of the present results with previous studies is also provided.

EXPERIMENTAL SETUP AND INSTRUMENTATION

Wind Tunnel

A wind tunnel facility similar to the one used in previous compact exchanger analysis [7] was modified to accept exchanger prototypes with approximately 0.25 m^2 frontal area and to provide two-dimensional flow as free of vibration and turbulence as reasonably possible for exchanger performance studies. A schematic diagram of the wind tunnel is shown in Fig. 1. The system is designed to suck room air over the finned side of the exchanger while circulating hot water through the tubes. The tunnel, made of 0.5 mm thick galvanized sheet metal, was a square duct 50 cm × 50 cm in cross section and 1100 cm in overall length. To avoid the flow of dust particles into the system, the entrance section contains two 100 cm × 100 cm screens of 10 meshes per cm, and 0.2 mm diameter steel wire cloth.

Through a 50 cm long Zanker-type flow straightener [8], air flows approximately 500 cm in a straight horizontal

Experimental Thermal and Fluid Science 1993; 6:263–272

0894-1777/93/$6.00

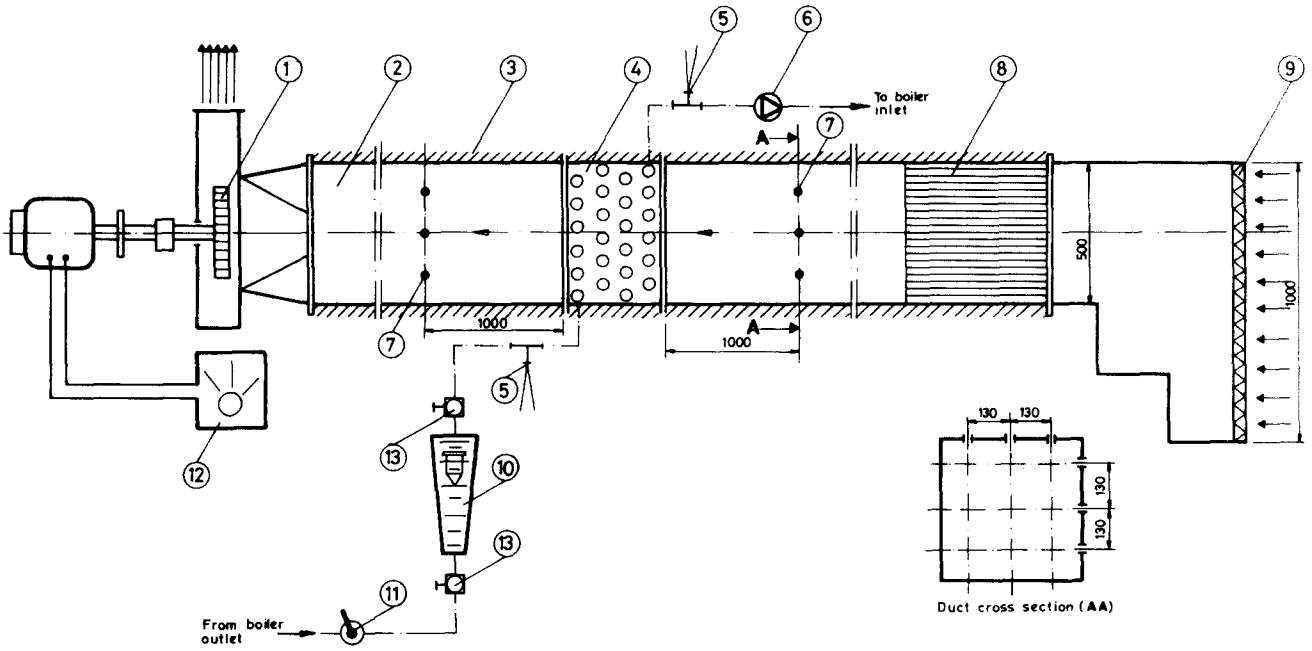

Figure 1. A schematic diagram of the experimental apparatus and the instrumentation. 1, Blower; 2, wind tunnel; 3, insulation; 4, test exchanger; 5, thermocouple; 6, pump; 7, air-side measurement point; 8, straightener; 9, screen; 10, rotameter; 11, main valve; 12, electronic variator; 13, flow adjustment valve.

duct before reaching the test section. As depicted in Fig. 1, the duct wall surfaces 100 cm downstream and upstream of the test section are furnished with a total of 12 holes 10 mm in diameter. Axisymmetric with these holes, cylindrical Teflon elements, 10 mm I.D., are attached to the tunnel to provide access holes for the velocity probe. Air leaving the metering section flows through a sheet metal transition section and enters the fan. At the fan exit, the air is discharged to the outdoors. To minimize heat loss to the surroundings, the tunnel outer surface is insulated with a 2 cm thick glass-wool layer. Additionally, being supported by stands of perforated steel plates, the duct system is elevated 50 cm above the floor level of the laboratory room.

Power for the wind tunnel was provided by a Sontec Model 6938 fan driven by a 3 kW ac motor. The motor was in turn powered by an electronic variac; a three-phase motor control unit and the fan speed could be varied in a continuous manner from 0 to 1350 rpm. Thus it was possible to alter the tunnel air velocity in the range of 0–15 m/s. A digital display panel indicated the fan rotational speed.

Hot Water System

The hot water system consists of a boiler of 115 kW heating capacity, a circulating pump, a flow-metering unit, and the test exchanger. All components of the system were interconnected with insulated steel piping 25 mm in diameter. Thus, a closed circuit between the boiler and the test exchanger was established. The boiler contained 1500 liters of water and was fired by a burner. A Honeywell thermostat, located at the exit, kept the water temperature at a preset value of 80°C. The burner was controlled by the thermostat so that the exit water temperature was allowed to vary within ± 3°C of the preset value. Owing to the large capacity of the boiler tank, stable temperatures at the exit were achieved.

Test Heat Exchanger

Figure 2 shows the fin layout and the tube circuit arrangement of the exchanger that was studied in this experiment. Table 1 presents the geometrical parameters of all the tested coils. Each core had flat, continuous 0.2 mm thick aluminum fins with collars. The copper tubes of 0.5 mm wall thickness, a product of Wieland Corporation, were manufactured with ± 0.06 mm tolerance on the outside diameter. After assembly, the tubes were mechanically expanded into the fins and tube sheets. The mechanical bond between the fins and tubes was checked and judged to be quite tight, and a negligible fin–tube thermal contact resistance was secured. The return bends were manually soldered to the tube extensions. Thus, the tubes of each row were interconnected, and four identical multipass crossflow circuits connected in parallel were obtained.

Avoiding any possible clogging, each circuit was tested with pressurized air. Then the 25 mm steel tubing headers for the supply and collection of hot water through the circuits were attached. The tube sheets, which form a casing for the core and possess mounting holes on their periphery, were fabricated of galvanized steel sheet 0.5 mm thick.

Instrumentation

The hot water supply to the test section was metered by an ASA glass tube variable-area rotameter. The meter had a sensitivity of 1 liter/min per cm of bob displace-

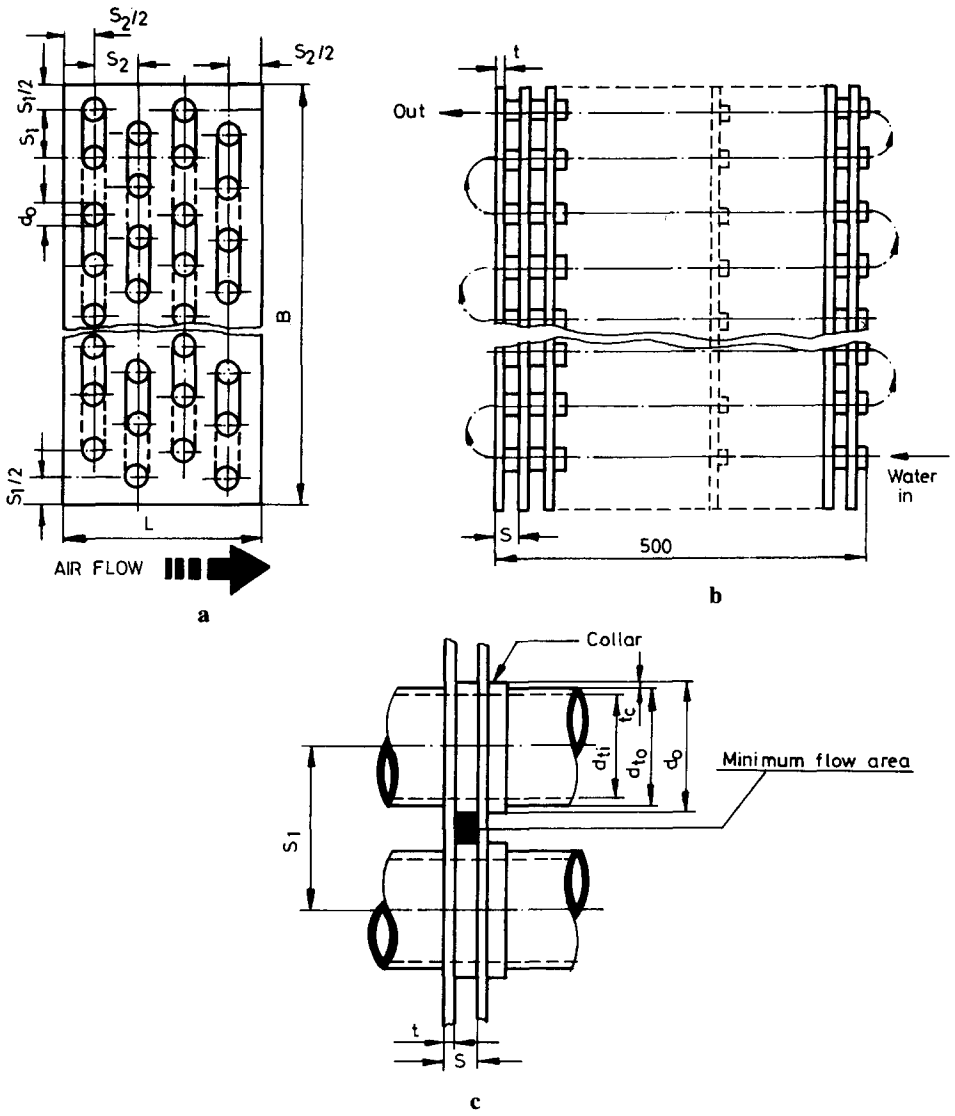

Figure 2. (a). The heat exchanger characteristic geometry. (b) The multipass water flow circuit. (c). A magnified view of the tube–fin combination.

ment and was calibrated to be accurate within ±2% of the full range. The flow rate adjustment through the coil was accomplished by two gate valves located at the inlet and outlet of the rotameter.

The water temperatures were recorded by a Sonde temperature indicator set. Measuring temperatures in the range of −15°C to 90°C, the probes of the instrument were 24 AWG copper-constantan (Type T) thermocouple elements enclosed in a 10 mm O.D. stainless steel protection tube. Vinyl-insulated lead wires terminate at the socket junction of the analog indicator. The set was calibrated by placing the probes in a variable-temperature bath whose temperature was measured by a precision thermometer. As illustrated in Fig. 3, the probes were housed in wells in the exchanger headers, and their positions were fixed by fittings. To attain uniform water-temperatures, a mixer, made of a perforated shim, was located upstream of each probe.

The airstream velocity and temperature measurements were obtained with a TSI Model 1650-1 hot-wire constant-temperature anemometer. The extendable probe wand had a sensing tip 4.7 mm in diameter. Using the sensor as a resistance thermometer, the instrument could also be used to measure air temperature. As specified by the manufacturer, the accuracy in velocity measurements was ±2%, and in temperature measurements ±0.8% of full scale.

A barometer indicated the ambient pressure, and a psychrometer was used to measure the dry bulb and wet bulb temperatures of the room air.

EXPERIMENTAL PROCEDURE AND DATA REDUCTION

The heat exchanger with specified surface geometry was installed in the wind tunnel in such a manner that the horizontal position was checked with a level, and the tunnel connections were sealed with epoxy. For some

Table 1. Geometric Parameters of the Tested Coils

Coil Type	Tube Diameter d_{to} (mm)	Coil Height B (mm)	Flow Length L (mm)	Transverse Pitch s_1 (mm)	Long. Pitch s_2 (mm)	Fin Spacing s_F (m^{-1})	Exchanger Finning Factor ϵ	Tubes per Row n	Number of Rows N
1	16.3	500	139	40	34.67	454	23.24	12	4
2	16.3	500	139	40	34.67	312	15.81	12	4
3	16.3	500	139	40	34.67	238	12.12	12	4
4	9.52	480	104	30	26	454	23.53	16	4
5	9.52	480	104	30	26	312	16.00	16	4
6	9.52	480	104	30	26	238	12.33	16	4
7	9.52	482	88	25.4	22	454	16.44	19	4
8	9.52	482	88	25.4	22	312	11.28	19	4
9	9.52	482	88	25.4	22	400	14.43	19	4
10	12.5	493	127	31.75	32	454	22.81	15	4

configurations, the exchanger height was less than the tunnel dimensions, and the bypass flow was eliminated by a thin layer of foam plastic sandwiched between the edges of the fins and the casing. Upon completion of the water-side links, the coil was completely insulated with a 5 cm thick layer of glass wool. The air in the water circuit was purged out through the purging plugs. The upstream and downstream valves of the rotameter were adjusted such that the average water velocity through the coil tubes was approximately 0.5 m/s, and then the tunnel blower was turned on and the air velocity was adjusted to a desired value. The water inlet and outlet temperatures were periodically checked, and equilibrium was assumed to exist if no appreciable deviation in water temperature change was observed for the last 15 min prior to data recording.

As shown in Fig. 4, the tunnel cross section was divided into six segmental areas, and in accordance with the log-linear rule [8] the velocity and temperature of the airstream at a total of 21 grid points were measured. The

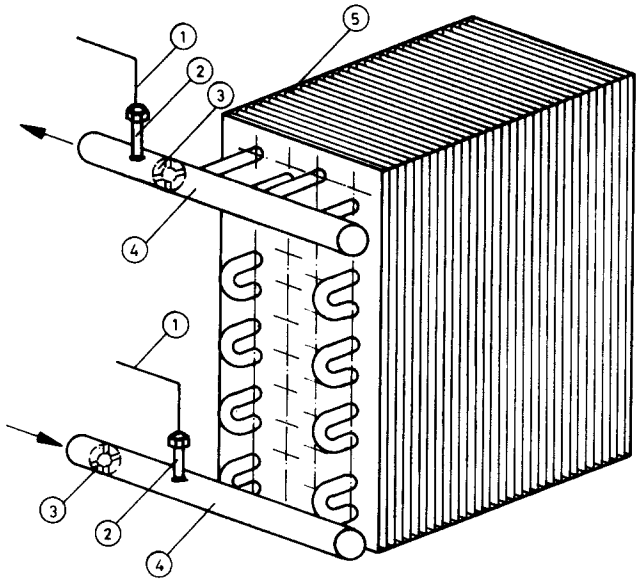

Figure 3. A schematic diagram of the water-side flow distribution and the instrumentation. 1, Thermocouple; 2, thermowell; 3, mixer; 4, header; 5, test exchanger.

air-side mass flow rate was then determined as follows:

$$M = (\rho aV)_o + \tfrac{1}{4}\sum_{j=1}^{5} a_j \sum_{k=1}^{4} (\rho_k V_k)_j \qquad (1)$$

where the subscript k indicates the four velocity values at a particular segmental area a_j.

Similarly, the air enthalpy at the exit is

$$H_e = (\rho aVc_pT)_o + \tfrac{1}{4}\sum_{j=1}^{5} a_j \sum_{k=1}^{4} (\rho_k c_{p,k} V_k T_k)_j \qquad (2)$$

Because of the uniform temperature distributions at the inlet of the test section, the inlet air enthalpy is

$$H_{\text{in}} = Mc_{p,\text{in}}T_{\text{in}} \qquad (3)$$

The difference between Eqs. (2) and (3) yields the rate at which heat was gained by the air and was compared with the heat loss of the water. In most experimental runs, the heat rate difference between the two sides was within $\pm 5\%$ range of the water-side heat rate. In calculating the exchanger overall conductance, UA, however, the arithmetic average of the air- and water-side heat rates was taken into account. The uncertainties in the measured properties were estimated to be as in Table 2. With the uncertainties given in Table 2, and over the indicated ranges, the method of Kline and McClintock [9] was employed to evaluate the uncertainties of the experimental results. For a typical case, the average heat flow rates were found to be within 6.1%, the Reynolds numbers within 8.1%, and the j factors within 11.2% of the reported values.

By the Colburn analogy [10], the functional relationship $\text{Nu} = \phi(\text{Re}, \text{Pr}, \text{flow geometry})$, suggested by the governing equations becomes

$$\text{Nu} = C\,\text{Re}^m\,\text{Pr}^{1/3}\epsilon^n \qquad (4)$$

for Prandtl numbers in the range $0.5 < \text{Pr} < 100$. For the test cases, it was calculated that $\text{Pr} \sim 0.7$. In this study, the maximum velocity, that is, the velocity at the minimum flow area, was used for the Reynolds number characteristic velocity, and as given by Eq. (A1) in the Appendix the characteristic diameter included the collar thickness. Thus, the Reynolds number is

$$\text{Re} = G_m d_o/\mu_b \qquad (5)$$

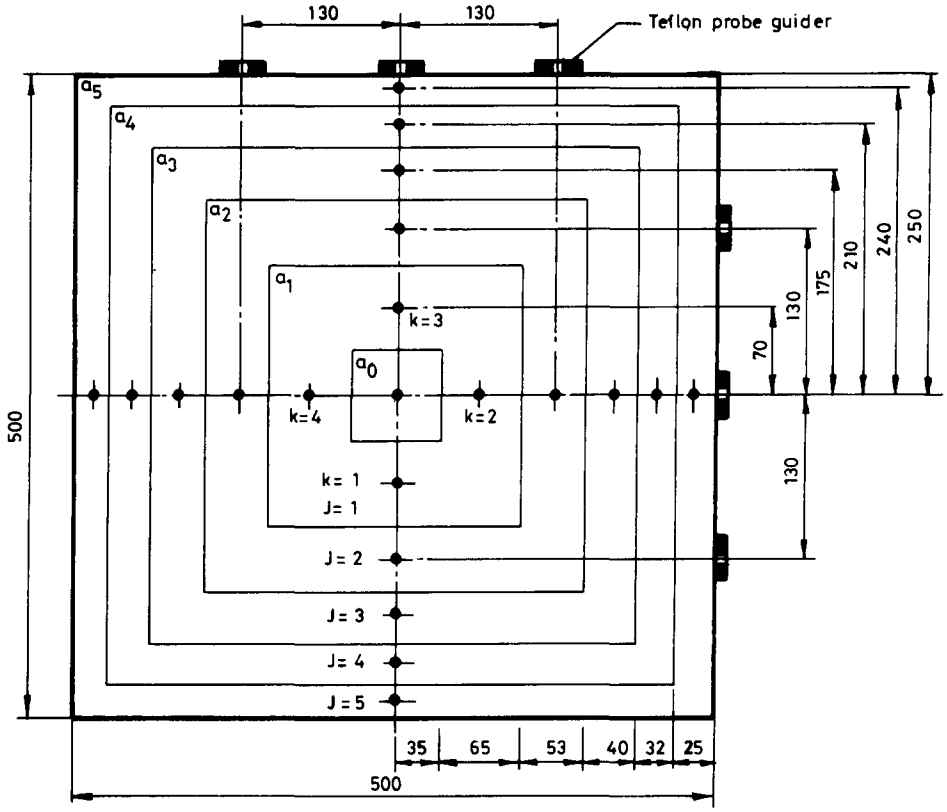

Figure 4. The wind tunnel cross section illustrating the velocity and temperature measurement points.

where $G_m = M/A_{\min}$. In Eq. (4), as suggested by McQuiston [6], the flow geometry effects are represented by the exchanger finning factor

$$\epsilon = A_o/A_{to} \tag{6}$$

Combining the definition of the Stanton number and the sensible Colburn j factor yields

$$j = \mathrm{Nu}/(\mathrm{Re}\,\mathrm{Pr}^{1/3}) \tag{7}$$

Hence, it is apparent from Eq. (4) that

$$j = C\,\mathrm{Re}^{m-1}\epsilon^n \tag{8}$$

A multiple linear regression analysis of the experimental data permits the determination of the coefficients of Eq. (8).

Determination of h_o, however, is made by first determining an overall heat transfer coefficient from the relationship

$$Q = UAF\,\Delta T_m \tag{9}$$

Table 2. Experimental Uncertainties

Property	*Uncertainty*	*Range*
Water flow rate	±0.5 liter/min	≤ 28 liters/min
Inlet water temp.	±0.8°C	77–84°C
Water temp. difference	±1°C	10–41°C
Outlet air temp.	±0.8°C	29.2–67.8°C
Inlet air temp.	±0.5°C	7–19.5°C
Air velocity	±0.06 m/s	0–3 m/s
Air velocity	±0.2 m/s	2.5–12.5 m/s
Probe access length	±1 mm	25–475 mm

where ΔT_m is the logarithmic mean temperature difference calculated from the measured inlet and outlet water and air temperatures and F is the correction factor applied to the mean temperature difference [11]. The overall heat transfer coefficient is related to the desired air-side film coefficient by

$$\frac{1}{U_o} = \frac{A_o}{A_i}\left(\frac{1}{h_i}\right) + \frac{1}{\eta_o}\left(\frac{1}{h_o}\right) + R_c \tag{10}$$

where R_c is the combined resistance of the tube wall and the collar. As this has a value of 3.8×10^{-5} m$^2 \cdot$ °C/W, it was neglected compared to the other terms of Eq. (10).

The surface efficiency, η_o, is given by

$$\eta_o = 1 - \frac{A_f}{A_o}(1 - \eta_f) \tag{11}$$

Here, η_f is the fin efficiency and is calculated as in Ref. 13.

Owing to the existence of fully developed turbulent flow inside the tubes, the water film coefficients h_i were determined from the Dittus-Boelter correlation [14],

$$\mathrm{Nu}_i = 0.023\,\mathrm{Re}_i^{0.8}\,\mathrm{Pr}^{0.4} \tag{12}$$

Since the surface efficiency η_o depends upon h_o, an iterative determination of h_o from measured data was required.

RESULTS AND DISCUSSION

Preliminary heat transfer measurements were undertaken to check the instrumentation and methodology used in this study. There are a number of finned-tube configura-

Table 3. Geometric Properties of the Compared Coils

Fig. No.	*Ref.*	*Finning Factor* ϵ	*Hydraulic Diameter* d_h *(mm)*	*Free-Flow Area Ratio* σ
5	This study	11.28	3.8	0.571
	[12]	11.23	3.9	0.579
6	This study	14.43	3.0	0.560
	[12]	13.88	3.1	0.572
7	This study	16.44	2.6	0.553
	[3]	17.54	2.7	0.543
8	This study	15.81	3.8	0.546
	[3]	12.34	3.9	0.555
9	This study	23.24	2.6	0.529
	[5]	21.41	2.7	0.540

tions for which experimental data are available that can provide a basis for comparison with the results reported here. The related geometrical properties of the compared coils are presented in Table 3. The compared sensible heat transfer coefficients are given in Figs. 5–9 and are consistent with the literature values. The coil hydraulic diameter, as defined by Eq. (A13) of the Appendix, is used in determining the Reynolds numbers.

In general, the trends for the Colburn j factors are in agreement with those documented in the literature. In Fig. 6, owing to experimental uncertainties at low flow rates, a maximum of 25% deviation in the results is noted. As the Reynolds number increases, however, the discrepancy decreases. A similar trend is observed in Fig. 8. In this figure, the distinct behavior of the two compared coils is attributable to a 22% discrepancy in the finning factors. As given by Eq. (8), the finning factor ϵ, representing the surface geometry, directly influences the j factor, and such deviations as those in Fig. 8 are expected to occur. In Fig. 9, although the proper trend is exhibited, Elmahdy's correlation for his test heater consistently shows higher values for the heat transfer. As illustrated in Fig. 5 of Ref.

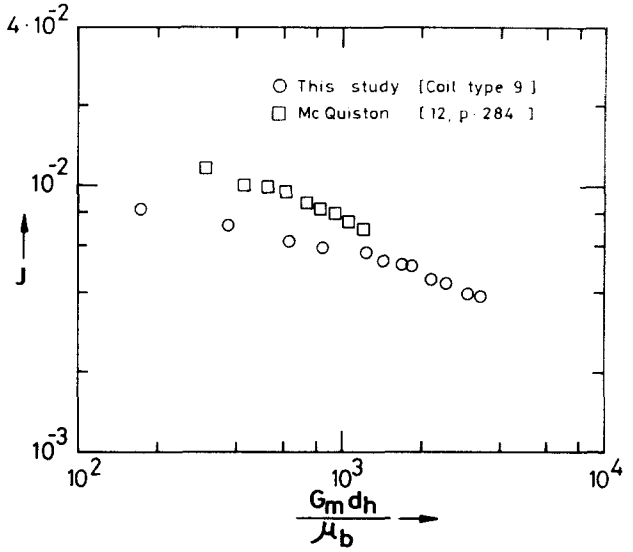

Figure 6. j versus Re_h. Comparison of present heat transfer results with the data of McQuiston, $\epsilon = 14.43$.

5, Elmahdy reported an overestimation to data. In addition, the coil tested by Elmahdy had eight rows in the flow direction. Then the higher j factors in his work are also consistent with the conclusiosn of Rich [4].

Reducing the measured values for a total of 110 experimental runs to j factors as defined by Eq. (7), all the data points are shown in Fig. 10 . The mean line through the 10 geometrical combinations of ϵ was obtained by a least squares curve fit. In the least squares treatment, the data points with Reynolds numbers below 500 were excluded because of low Reynolds number effects, conduction and natural convection, which preclude a boundary type of analysis. Accordingly the following correlation was obtained.

$$j = 0.15\,\mathrm{Re}^{-0.28}\epsilon^{-0.362} \tag{13}$$

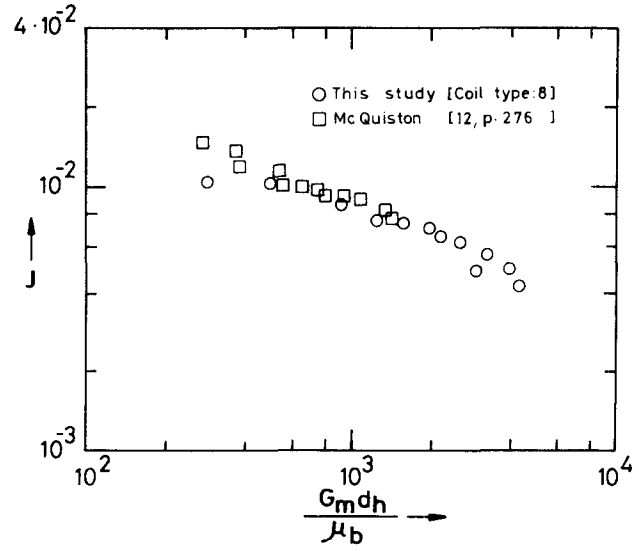

Figure 5. j versus Re_h. Comparison of present heat transfer results with the data of McQuiston, $\epsilon = 11.28$.

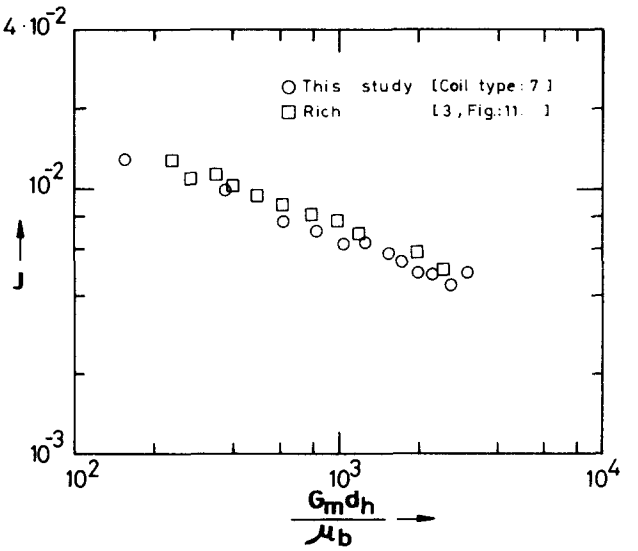

Figure 7. j versus Re_h. Comparison of present heat transfer results with the data of Rich, $\epsilon = 16.44$.

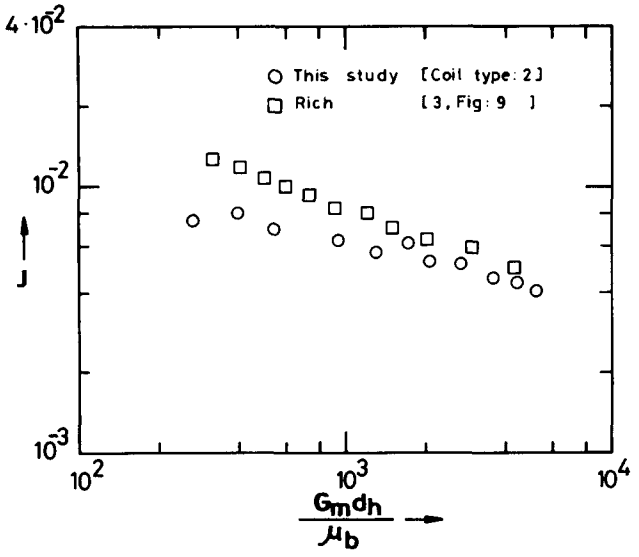

Figure 8. j versus Re_h. Comparison of present heat transfer results with the data of Rich, $\epsilon = 15.81$.

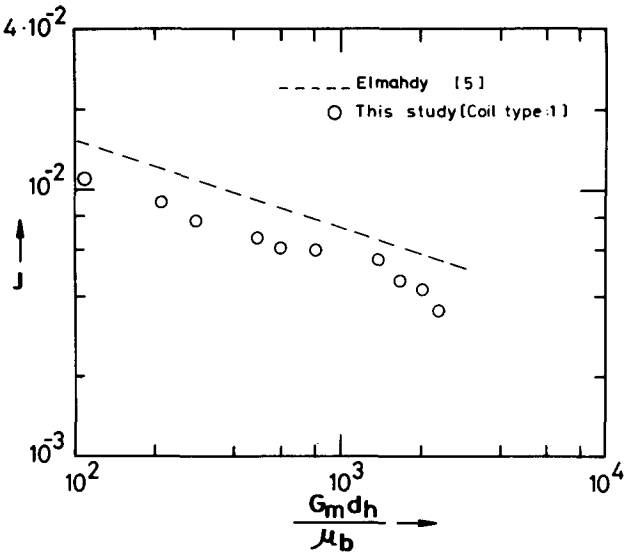

Figure 9. j versus Re_h. Comparison of present heat transfer results with Elmahdy's correlation, $\epsilon = 23.24$.

in which $500 < Re < 30{,}000$ and $11.2 \leq \epsilon \leq 23.5$. The thermophysical properties in Eq. (13) are evaluated at the arithmetic average of the air inlet and outlet bulk temperatures.

A search of the literature revealed that attempts have been made to obtain generalized correlations for the heat transfer coefficients related to the subject of the present study by McQuiston [6] and more recently by Webb [15]. In McQuiston's analysis, however, the channel effect of the fins was neglected, and the flows over the finned tube surface and over the bank of bare tubes were assumed to be similar. Then, for Reynolds numbers in the range 100–4000, the exponent $m - 1$ of Eq. (8) was -0.4 [14]. Because of the presence of fins, the flow along the flat plate is superimposed on the flow around the tubes. Especially at high Reynolds numbers, the fin effect becomes stronger. Hence, the exponent $m - 1$ should assume a value between -0.4 and -0.2, where the lower limit represents the tube bank and the upper limit the channel flows. Applying a multiple regression technique to the data of 16 flat-plate heat exchangers, Gray and Webb [16] developed a correlation in which the Reynolds number exponent was -0.328. In this study, the j-factor slope is determined to be -0.28. Such a slope value appears to be in agreement with the strong channel effect of fins on the flow at high Reynolds numbers. Elmahdy and Biggs [5] reported slopes ranging from -0.36 to -0.30 for several geometrically different exchangers. The slope discrepancy may be due to the distinct definition of characteristic length in their work.

The present data for coil types 8 and 4 are compared with the correlation stated by Webb [16, eq. (5)] in Fig. 11. Starting from the first distribution for $\epsilon = 11.28$, which

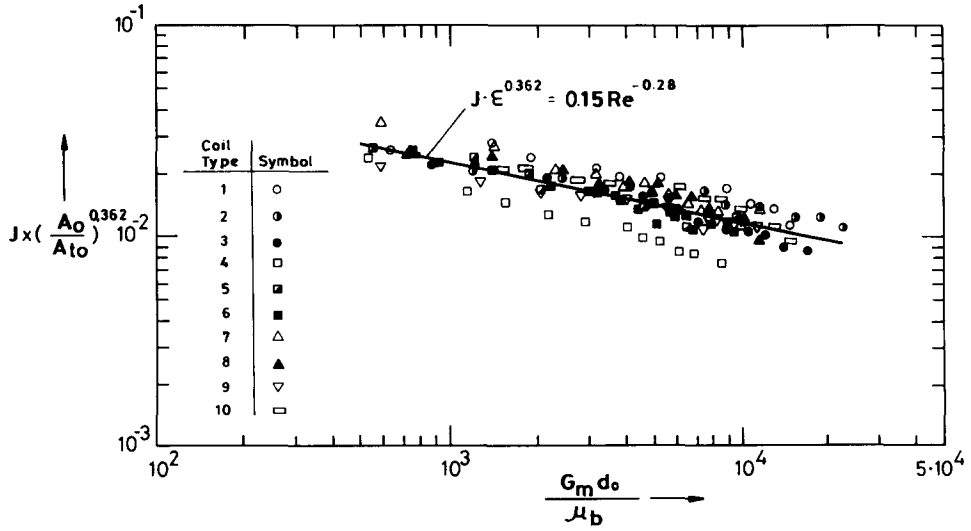

Figure 10. Average convective heat transfer as a function of Reynolds number, $11.2 \leq \epsilon \leq 23.5$.

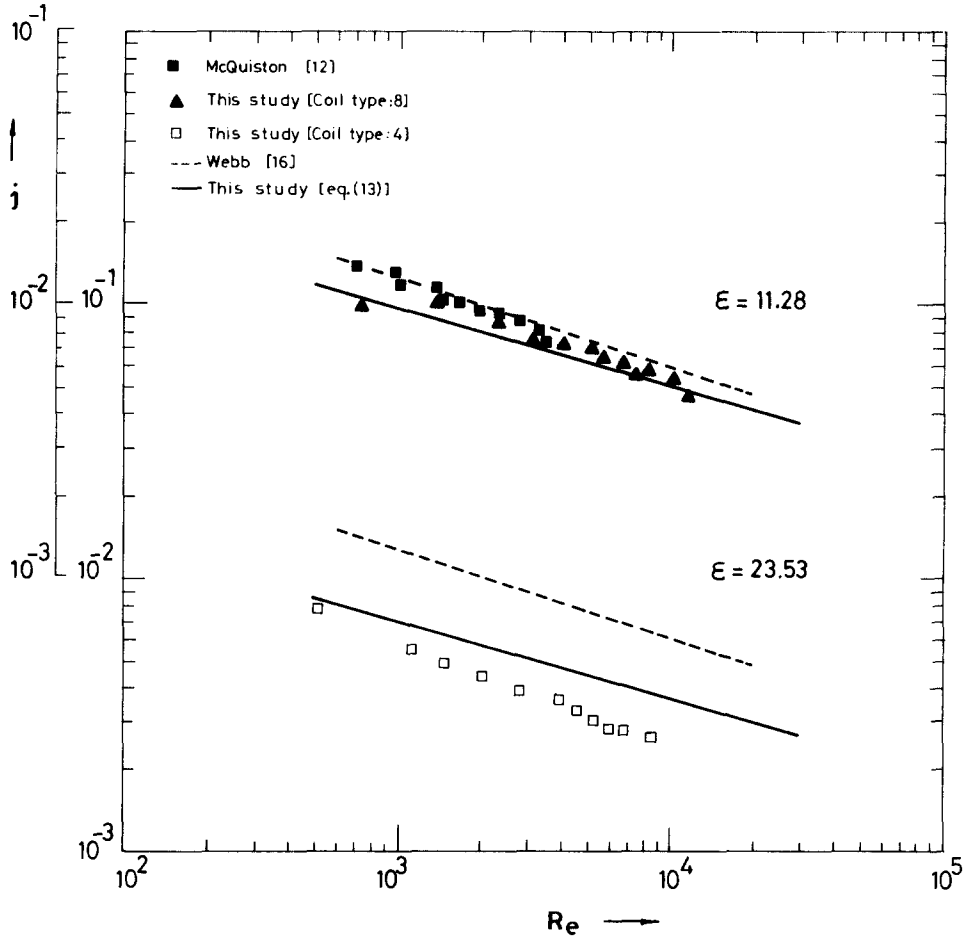

Figure 11. Comparison of present correlation with Ref. 16 for the data for coil types 8, 4, and McQuiston [12].

also contains the data of McQuiston [12], it should be noted that Webb's correlation represents the results with reasonable accuracy at low Reynolds numbers. As the Reynolds number increases, however, the correlation line diverges from the data points. The percentage of error in the j-factor representation is defined as

$$E = \frac{j_{\text{analytical}} - j_{\text{experimental}}}{j_{\text{analytical}}} \times 100 \qquad (14)$$

where $j_{\text{analytical}}$ is the j factor calculated by using any of the stated correlations. Then, typically at Re = 12,000, Webb's correlation is found to deviate by 29.5% while Eq. (13) deviates by 8.2%. In the second distribution for $\epsilon = 23.53$, the geometric ratios for coil type 4 are $s_1/d_0 = 3.02$ and $s_2/d_o = 2.62$ and exceed the range of validity of Webb's correlation. As shown in Fig. 11, Webb's correlation exhibits a large discrepancy with the present data. It is quite difficult to interpret this particular manifestation. However, as noted by Webb [16], the small influence of fin spacing, especially at high flow rates, is probably misleading. Considering a limiting case for which s_1/d_o and s_2/d_o are assumed to have large values and $s/d_o \ll 1$, then it would not be appropriate to neglect the channel effect of fins on the flow, and disregarding this effect may lead to higher j-factors. In Fig. 11, at Re = 9000, Eq. (13) displays a maximum of 31% error to the data for coil type 4.

PRACTICAL SIGNIFICANCE

The results of this study represent the first phase of a research program motivated by the need to develop an improved understanding and characterization of forced convection heat transfer on compact plate-fin heat exchanger surfaces. In addition to covering only restricted variations in the exchanger surface geometry, existing correlations in the engineering literature are applicable to only a limited range of Reynolds numbers. However, heat exchanger designers and analysts require a correlation with reasonable accuracy validated for a wide range of Reynolds numbers and for diversified geometrical conditions. The present study aims to fulfill this requirement. The exchanger finning factor obtained by means of Eq. (A10) can be applied in Eq. (13) to predict the performance characteristics of untested but geometrically similar heat exchangers, provided they are operated in the Reynolds number range 500–30,000.

CONCLUSIONS

In the experiments, the geometrical parameters of the 10 tested coils were varied in the ranges of $2.39 < s_1/d_o <$

3.15, $2.07 < s_2/d_o < 2.67$, and $0.131 < s/d_o < 0.425$. The Reynolds number presentation is based on the tube outside diameter including the collar thickness. As described in the Appendix, all the geometrical properties are embodied in a single parameter, the finning factor ϵ. The performance of a flat fin and round tube heat exchanger is best expressed in terms of a Colburn j factor, and a relation between this and the Reynolds number, the finning factor, is then sought.

A strong dependence of the heat transfer coefficients on the finning factor ϵ is noted. As the value of ϵ increases, the general behavior of the exchanger, as expected, is that the j factor decreases. The fin density s_F is a major parameter in the representation of ϵ (Eq. (A10)), and the more dense the fins are, the more pronounced the channel effect is.

Although Eq. (13) represents the data points with a correlation coefficient of 0.93, care should be exercised in using the results. Of all the data in Fig. 10, 71.8% lie within a $\pm 10\%$ dispersion band around the mean line. Out of 110 experimental data, however, five data points are found to scatter deviations of $+30\%$ and 14 by -30% which also indicate the upper and lower limits of error for Eq. (13).

The work reported here is part of a research project sponsored by Turbo-Therm Heat Exchangers Manufacturing Corporation. Their financial and technical support is gratefully acknowledged.

APPENDIX. HEAT EXCHANGER GEOMETRY

In order to relate the finning factor to the geometry of the heat exchanger, it is necessary to consider the following definitions for the flat-fin, crossflow, staggered-tube exchanger. Referring to Fig. 2, denoting the tube outside diameter by d_{to} and the collar thickness by t_c, then the characteristic dimension becomes

$$d_o = d_{to} + 2t_c \tag{A1}$$

The relation between the number of tubes per row, n, the transverse pitch s_1, and the exchanger height B is

$$B = ns_1 \tag{A2}$$

Similarly, the number of tube rows, N, the longitudinal tube pitch s_2, and the flow length L are related as

$$L = Ns_2 \tag{A3}$$

Then the minimum flow area per unit length and the exchanger frontal area per unit length are

$$A_{\min} = n(s_1 - d_o)(1 - ts_F) \tag{A4}$$

and

$$A_{\text{fr}} = ns_1 4s \tag{A5}$$

The parameter s_F is termed the fin density and has units of fins per unit length. The ratio of Eqs. (A4) and (A5) becomes

$$\sigma = (1 - d_o/s_1)(1 - ts_F) \tag{A6}$$

The finned area per unit length and the tube outside area with collar per unit length are given by

$$A_f = Nn\frac{\pi d_o^2}{2}\left[\frac{4}{\pi}\left(\frac{s_1}{d_o}\right)\left(\frac{s_2}{d_o}\right) - 1\right]s_F \tag{A7}$$

and

$$A_{to} = Nn\pi d_o(1 - ts_F) \tag{A8}$$

Then the total outside surface area per unit length is

$$A_o = Nn\pi d_o\left\{(1 - ts_F) + \frac{d_o}{2}\left[\frac{4}{\pi}\left(\frac{s_1}{d_o}\right)\left(\frac{s_2}{d_o}\right) - 1\right]s_F\right\} \tag{A9}$$

Together with Eqs. (A9), (A8), and (A6), the definition of the finning factor ϵ yields

$$\epsilon = 1 + \left[\frac{4}{\pi}\left(\frac{s_1}{d_o}\right)\left(\frac{s_2}{d_o}\right) - 1\right]\left(1 - \frac{d_o}{s_1}\right)\left(\frac{d_o s_F}{2\sigma}\right) \tag{A10}$$

Furthermore, the total inside area of the coil tubes per unit length is

$$A_i = Nn\pi d_i \tag{A11}$$

Having thus described the characteristic geometry of the heat exchanger, it is apparent that the hydraulic diameter is defined as

$$d_h = 4\sigma A_{\text{fr}} L/A_o \tag{A12}$$

In terms of the geometrical properties of the exchanger, the following relation for the hydraulic diameter can be derived:

$$d_h = \frac{8\sigma}{\pi}\left(\frac{(s_1/d_o)(s_2/d_o)}{\frac{2}{d_o}(1 - ts_F) + \left[\frac{4}{\pi}\left(\frac{s_1}{d_o}\right)\left(\frac{s_2}{d_o}\right) - 1\right]s_F}\right) \tag{A13}$$

NOMENCLATURE

- A surface area, m^2
- a segmental area of wind tunnel cross section, m^2
- B exchanger height, m
- c_p specific heat, kJ/(kg · °C)
- d diameter, m
- E percentage of error [Eq. (14)], dimensionless
- F correction to logarithmic temperature difference, dimensionless
- G_m mass flux, kg/(m^2 · s)
- H air-side enthalpy, W
- h heat transfer coefficient, W/(m^2 · °C)
- j Colburn j factor [$= (h_o/G_m c_p)\text{Pr}^{2/3}$], dimensionless
- k thermal conductivity, W/(m · °C)
- L flow length, m
- M mass flow rate, kg/s
- m Reynolds number exponent [Eq. (4)], dimensionless
- N number of tube rows, dimensionless
- n number of tubes per row, dimensionless
- Nu Nusselt number ($= h_o d_o/k_b$), dimensionless
- Pr Prandtl number ($= \mu_b c_p/k_b$), dimensionless
- Q heat transfer rate, W

Re Reynolds number ($= G_m d_o/\mu_b$), dimensionless
s fin spacing, m
s_1 transverse tube pitch, m
s_2 longitudinal tube pitch, m
s_F fin density, fins/m
T temperature, °C
ΔT_m logarithmic mean temperature difference, °C
t fin thickness
t_c collar thickness, m
U overall heat transfer coefficient, $W/(m^2 \cdot °C)$
V velocity, m/s

Greek Symbols

Δ difference
ϵ exchanger finning factor [Eq. (6)], dimensionless
η efficiency
μ dynamic viscosity, $kg/(m \cdot s)$
ρ density, kg/m^3
σ minimum to frontal area ratio, [Eq. (A13)], dimensionless

Subscripts

b bulk
e exit
f fin
fr frontal
h hydraulic
i inside
in inlet
j, k measurement points
min minimum
o outside
to tube outside

REFERENCES

1. Webb, R. L., Air-Side Heat Transfer in Finned Tube Heat Exchangers, *Heat Transfer Eng.*, **1**(3), 33–49, 1980.
2. McQuiston, F. C., Finned Tube Heat Exchangers: State of the Art for the Air Side, *ASHRAE Trans.*, **87**, 1077–1085, 1981.
3. Rich, D. G., The Effect of Fin Spacing on the Heat Transfer and Friction Performance of Multi-row, Smooth Plate Fin-and-Tube Heat Exchangers, *ASHRAE Trans.*, **79**(2), 137–145, 1973.
4. Rich, D. G., The Effect of the Number of Tube Rows on Heat Transfer Performance of Smooth Plate Fin-and-Tube Heat Exchangers, *ASHRAE Trans.*, **81**(1), 307–317, 1975.
5. Elmahdy, A. H., and Biggs, R. C., Finned Tube Heat Exchanger: Correlation of Dry Surface Heat Transfer Data, *ASHRAE Trans.*, **85**(2), 262–273, 1979.
6. McQuiston, F. C., Correlations of Heat, Mass and Momentum Transport Coefficients for Plate-Fin-Tube Heat Transfer Surfaces with Staggered Tubes, *ASHRAE Trans.*, **84**(1), 294–309, 1978.
7. Kays, W. M., and London, A. L., Heat Transfer and Flow Friction Characteristics of Some Compact Heat Exchanger Surfaces: Part 1. Test System and Procedure, *Trans. ASME*, **72**, 1075–1085, 1950.
8. British Standards, BS 1042, part 2A, 1973, pp. 38–59.
9. Kline, S. J., and McClintock, F. A., Describing Uncertainties in Single-Sample Experiments, *Mech. Eng.*, **75**, 3–8, 1953.
10. Colburn, A. P., A Method of Correlating Forced Convection Heat Transfer Data and a Comparison with Fluid Friction, *Trans. AIChE*, **29**, 174–210, 1933.
11. VDI-Wärmeatlas, *Berechnungsblätter für den Wärmeübergang*, VDI-Verlag, 1963.
12. McQuiston, F. C., Heat, Mass, and Momentum Transfer Data for Five Plate-Fin-Tube Heat Transfer Surfaces, *ASHRAE Trans.*, **84**(1), 266–293, 1978.
13. McQuiston, F. C., and Parker, J. D., *Heating, Ventilating, and Air Conditioning—Analysis and Design*, 3rd ed., Wiley, New York, pp. 555–562, 1988.
14. Incropera, F. P., and Dewitt, D. P., *Fundamentals of Heat and Mass Transfer*, 2nd ed., Wiley, New York, pp. 309–404, 1985.
15. Webb, R. L., Enhancement of Single-Phase Heat Transfer, in *Handbook of Single-Phase Convective Heat Transfer*, S. Kakaç, R. K. Shah, and W. Aung, Eds., Wiley, New York, Chapter 17, pp. 17.16–17.17, 1987.
16. Gray, D. L., and Webb, R. L., Heat Transfer and Friction Correlations for Plate Finned-Tube Heat Exchangers Having Plain Fins, *Heat Transfer 1986*, **6**, 2745–2750, 1986.

Received May 20, 1992; revised October 30, 1992